Electronic Supplementary Material (ESI) for Environmental Science: Advances.

Microwave catalytic activities of supported catalysts MFe_2O_4@CMT (M=Ni, Co) for dimethyl phthalate degradation

Wenli Qin[a], Xinyi Zhang[a], Zefei Chen[a], Xueya Liu[a], Manqing Ai[b], Pingping Zhang[b], Ying Ye[b], Zengling Ma[a1]

a National and Local Joint Engineering Research Center of Ecological Treatment Technology for Urban Water Pollution, College of Life and Environmental Science, Wenzhou University, Wenzhou, 325035, P.R. China

b Ocean College, Zhejiang University, Zhoushan, 316021, P.R. China

1. Materials information

Table S1 The content of the main elements in simulated seawater

Elements	Cl^-	Na^+	Mg^{2+}	SO_4^{2-}	Ca^{2+}	K^+	Br^-	others
Content (g L^{-1})	18.30	9.78	1.08	2.46	0.35	0.31	0.042	0.23

2. Pore structure analysis

Table S2 BET surface area and pore characteristics of PCCF and PCNF

Sample	Surface are (m^2 g^{-1})	Mesopore volume (cm^3 g^{-1})	Micropore volume (cm^3 g^{-1})	Average pore size (nm)
PCCF	8.995	0.231	0.058	8.36
PCNF	11.22	0.256	0.067	7.12

3. Permittivity and Permeability

The frequency dependence of EM parameters of ferrite/corncob composite were detected using vector network analyzer in the range of 1-18 GHz. As shown in Fig.

[1] Correrspoding author: Zengling Ma, Email: mazengling@wzu.edu.cn; Tel.: +86-0577-86689079; fax: +86-0577-86689079.

S1a and S1b, the real (ε') and imaginary permittivities (ε'') of CC were 22.74 - 206.14 and 63.25 - 194.33, respectively. The ε' and ε'' kept decreasing with the increasing of frequency. Consequently, their dielectric loss tangents (tan $\delta_e = \varepsilon''/\varepsilon'$, Fig. S1c) were generally invariant at 0.94 to 2.74. When coated with ferrite, the ε' were between 3.33 and 3.73 of PCCF, 3.62 and 3.83 of PCNF, which were smaller than that of CC; the ε'' of PCCF and PCNF fluctuated slightly with frequencies between 0.06 and 1.24. It is well known that $\varepsilon'' \approx \sigma/2\pi\varepsilon_0 f$ according to the free electron theory (Chen *et al.* 2012a), where σ is the conductivity of the sample; that is, higher ε'' values require higher conductivities. The ε'' values of ferrite/corncob composite are almost increased slightly with frequency, indicating that the poorer conductivity of ferrite/corncob composite than that of CC. Consequently, the tan δ_e value of ferrite/corncob composite increased to the maximum value at 2.74 of CC, 0.26 of PCCF, 0.10 of PCNF, where larger tan δ_e values show higher dielectric loss. It is indicated that the coating of ferrite/corncob will not increase the conductivity of the sample, resulted in PCCF and PCNF showed lower permittivity than CC.

Fig. S1d and S1e showed the frequency dependence of the relative complex permeability of ferrite/corncob composite. Because of the absence of magnetic components, the real (μ') and imaginary permeability (μ'') of CC were lower than that of PCCF and PCNF. Nevertheless, the μ' and μ'' values of PCCF showed slightly higher than PCNF exhibited highest value, the maximum μ' and μ'' value were 1.57 and 0.91, respectively. As a result, the magnetic loss tangent (tan $\delta_m = \mu''/\mu'$, Fig. S1f) of CC and PCNF were below 0.030, while the maximum magnetic loss tangent of

PCCF was 1.07. The complex permittivity and permeability values of ferrite/corncob composite suggest that the presence of ferrite will enhance the EM wave absorption, mainly induced by magnetic loss.

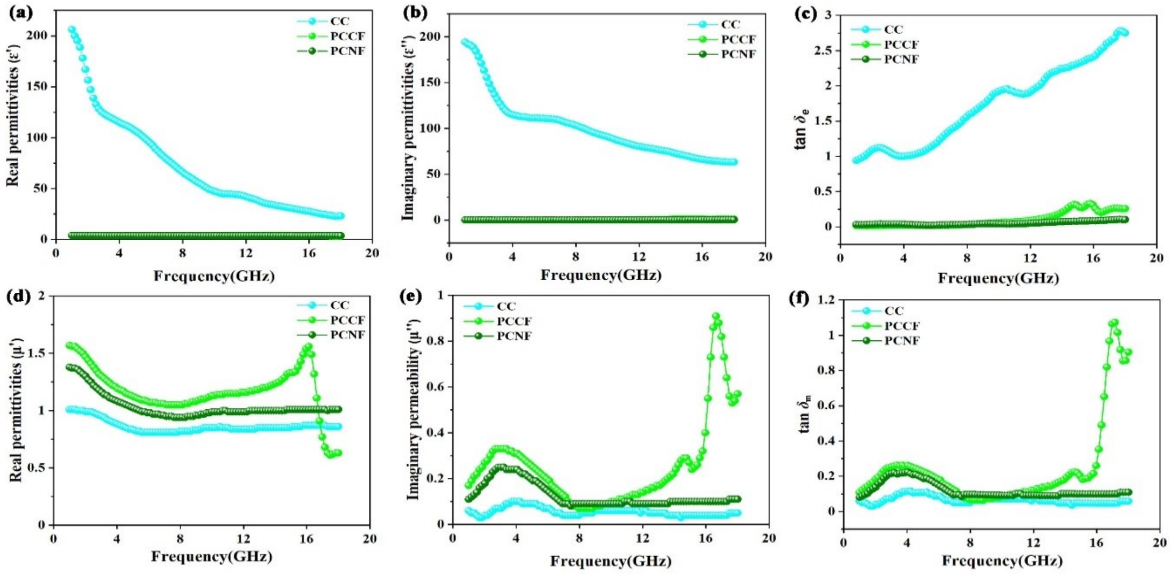

Fig. S1 Frequency dependence of (a) real permittivity, (b) imaginary permittivity, (c) dielectric loss tangent, (d) real permeability, (e) imaginary permeability, and (f) magnetic loss tangent of CC, PCCF, and PCNF with volume fraction of 50 % and thickness of 2 mm.

Table S3 The comparation between the different EM wave absorbing materials

	Thickness (mm)	**Maximum RL (dB)**
CC	2.72	-1.82
PCCF	1.82	-39.79
PCNF	6.47	-23.47
Porous Carbon fiber **(**Guan *et al.*, 2007**)**	2.9	-15.5
Porous Fe (Chen *et al.,* 2012b)	2.0	-21.9
Rice Husk Ash (Liu *et al.* 2014)	2.0	-12.5
Halloysite-Fe (Zhang *et al.*, 2014)	2.0	-0.8
Polypropylene/montmorillonite/polypyrrole (Moučka *et al.*, 2011)	100	-60.0

4. Degradation

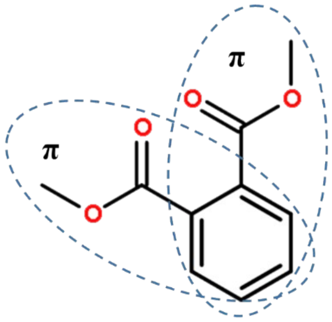

Fig. S2 Chemical structure of DMP

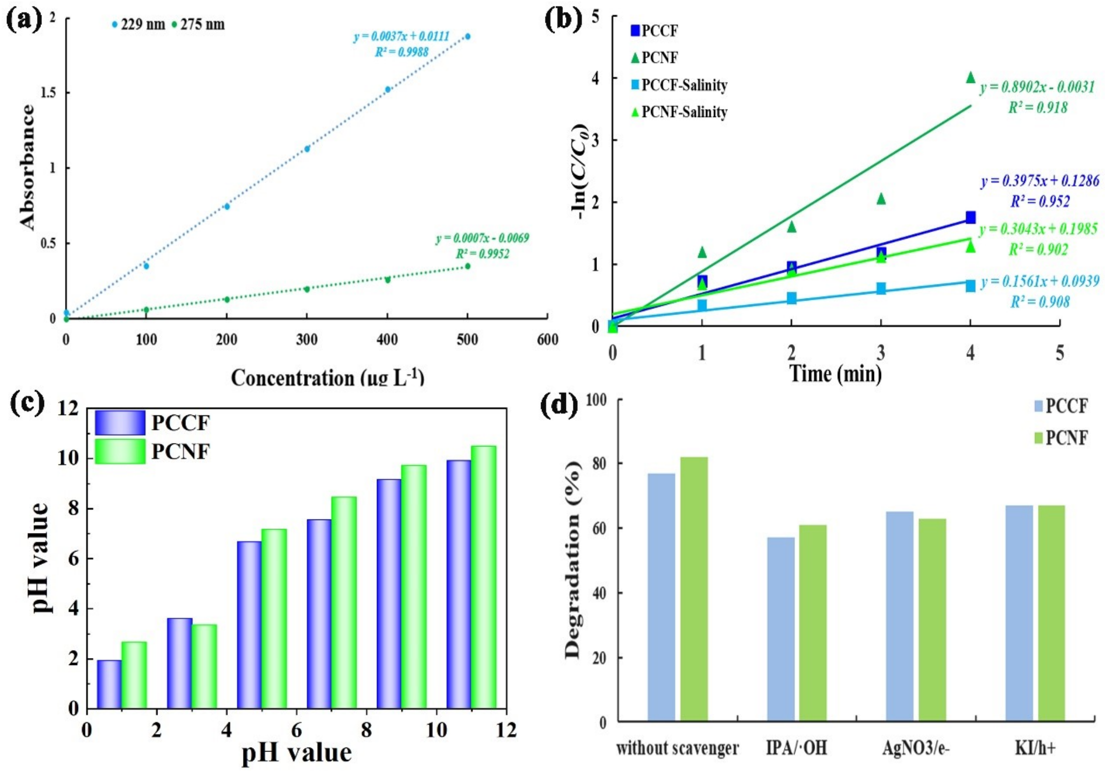

Fig. S3 (a) Standard curve of absorption peak of phenyl ester and benzene ring at 229 nm and 275 nm in the UV-Vis spectrum; (b) Kinetics studies of MW-induced degradation of DMP; (c) pH values of DMP solution after PCCF and PCNF microwave enhanced Fenton-like performance; (d) MW enhanced Fenton-like performance of PCCF and PCNF when hydroxyl radical quenching agent added after 1 min MW

Table S4 DMP degradation first-order kinetic reaction fitting kinetic constant

Catalyst	***k*** **(min^{-1})**
PCCF	0.3975
PCNF	0.8902
PCCF in salinity	0.1561

PCNF in salinity	0.3043

Table S5 Experimental details and the DMP removal rate of AOPs systems

Catalyst	Type of reaction	Catalyst dosage	DMP concentration ($mg\ L^{-1}$)	Time (min)	Degradation rate (%)	Reference
Hydroxylamine sulfate	Electro-Fenton (Fe^{2+}: 10 mM)	0.5 μM	10	20	96.7	Li, *et al.*, 2022
Graphene-WO_3	Dielectric barrier discharge plasma system	40 $mg\ L^{-1}$	10	60	90.60	Han, et al., 2022
Z-scheme iron oxide/mpg-C_3N_4/BiOBr/polythiophene	Photocatalytic	1.0 $g\ L^{-1}$	20	360	92	Li, et al., 2021
$CoFe_2O_4$@CMT	Microwave-assisted Fenton (H_2O_2: 200 $mg\ L^{-1}$)	2.0 $g\ L^{-1}$	500 $\mu g\ L^{-1}$	6	90	This paper
$NiFe_2O_4$@CMT	Microwave-assisted Fenton (H_2O_2: 200 $mg\ L^{-1}$)	2.0 $g\ L^{-1}$	500 $\mu g\ L^{-1}$	6	99	This paper

Table S6 Information on intermediates

Compound	**Structure**	**Formula**	**m/z**
DMP	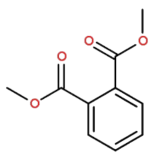	$C_{10}H_{12}O_4$	196
M1	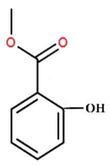	$C_8H_{10}O_3$	154
M2	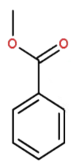	$C_8H_9O_2$	137
M3	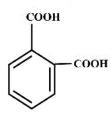	$C_8H_8O_4$	168

M4	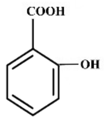	$C_7H_8O_3$	140
M5	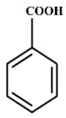	$C_7H_7O_2$	123
M6	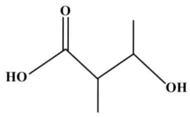	$C_5H_{10}O_3$	118
M7	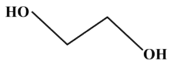	$C_2H_6O_2$	62

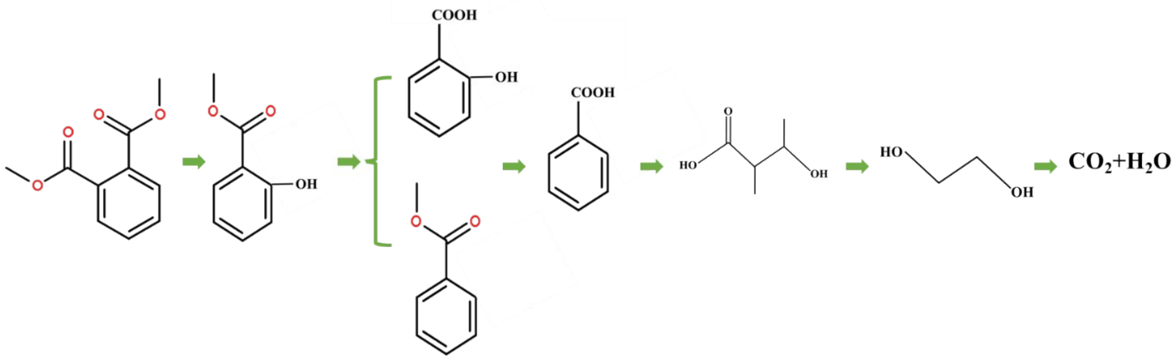

Fig. S4 The degradation pathway of DMP

4. XPS after reaction

Table S7 Surface elemental and group composition (%) of PCCF and PCNF before and after reaction.

	Catalyst	C 1s		O 1s		
		C-C/C=C	C-OH	H_2O	-OH	Fe-O
PCCF	Before	84.12	15.88	15.82	43.87	40.31
	After	81.74	18.26	3.29	51.02	45.69
PCNF	Before	82.36	17.64	14.32	47.36	38.32

	After	78.22	21.78	1.85	54.84	43.31

4. Health risk evaluation

The non-carcinogenic risk (HI) is which is calculated according to Eqs. S1-S4.

$$HI = \frac{CDI}{RfD} \tag{S1}$$

$$CDI_{drinking} = \frac{C \times U \times EF \times ED}{BW \times AT}$$

(S2)

$$CDI_{skin} = \frac{I \times A_{sd} \times FE \times ED}{BW \times AT \times f}$$

(S3)

$$I = 2 \times 10^{-3} \times k \times C \times (6 \times \tau \times TE/\pi)^{0.5} \tag{S4}$$

The meaning, reference value, and unit of each symbol in the formula was shown in Table S9.

When the HI value is less than 1, it indicates that the exposure dose does not cause non-carcinogenic risk to human body. An HI value greater than 1 indicates a non-carcinogenic health risk to humans.

Table S8 PAEs concentrations in surface water of rivers and lakes in some places in China and oversea

Site	**DMP**	**DEP**	**DiBP**	**DBP**	**BBP**	**DEHP**	**DOP**	**Reference**
Somme River Water, France	0.02~0.25	0.26~6.98	/	0.22~3.86	ND	5.16~20.8	ND	Net, *et al.,* 2014
Kaveri River, India	0.02	0.24	/	0.25	0.04	0.51	0.03	Selvaraj, *et al.*, 2015
False Creek Harbor, Spain	<0.5	<0.5	/	<0.5	<0.5	<0.5	<0.5	Mackintosh, et a 2009
Manzanares and Halama rivers, Spain	ND	ND	/	0.25~1.76	ND	ND	/	Dominguez-Moruec *et al.*, 2014
Xuanwu Lake, China	0.003~0.085	0.015~0.32	0.16~0.92	0.94~3.60	ND	0.087~0.63	ND	Zeng, *et al.*, 2008

Lake in Guangzhou, China	6.36~173.42	11.68~124.03	/		314.26~800.95	26.71~176.64	477.75~1299.54	7.24~64.15	Shen, *et al.*, 2010

Notes: 1) ND: not detected; 2) /: not determined.

Table S9 Meaning, reference value, and unit of each symbol in the formula

	Meaning	Reference value	Unit
CDI	Long-term daily intake	-	$mg\cdot(kg\cdot d)^{-1}$
RfD	Reference value	-	$mg\cdot(kg\cdot d)^{-1}$
SF	Slope factor of carcinogenic pollutants	-	$(kg\cdot d)\cdot mg^{-1}$
C	Contaminant concentration	-	$mg\cdot L^{-1}$
U	Daily drinking water quantity	1.825 (Male) 1.350 (Female) 1.000 (Children)	$L\cdot d^{-1}$
EF	Exposured frequency	365	$d\cdot a^{-1}$
ED	Exposured duration	74 (Male) 78 (Female) 12 (Children)	a
BW	Average weight	64.8 (Male) 55.1 (Female) 26.8 (Children)	kg
AT	Average exposured time	27010 (Male) 28470 (Female) 4380 (Children)	d
I	Amount of contaminants absorbed by skin	-	$mg\cdot cm^{-2}\cdot times^{-1}$
$\boldsymbol{A_{sd}}$	Surface area of the human body	17000 (Male) 15000 (Female) 8490 (Children)	cm^2
FE	Bathing frequency	0.3	$times\cdot d^{-1}$
TE	Bath time	0.4	h
f	Intestinal adsorption ratio	1	-

k	Skin adsorption parameter	0.001	$cm\cdot h^{-1}$
τ	Contaminant lag time	1	h
RfD	Reference dose	0.1	$mg\cdot(kg\cdot d)^{-1}$

Reference:

Chen, X, Lv, S, Zhang, P, Cheng, J, Liu, S, Ye, Y, 2012a. Fabrication and electromagnetic performance of micro-tubular nanocomposites composed of monodisperse iron nanoparticles and carbon. *Journal of Magnetism and Magnetic Materials,* 324(9):1745-1751.

Chen, X, Cheng, J, Lv, S, Zhang, P, Liu, S, Ye, Y, 2012b. Preparation of porous magnetic nanocomposites using corncob powders as template and their applications for electromagnetic wave absorption. *Composites Science and Technology,* 72(8):908-914.

Dominguez-Morueco, N, Gonzalez-Alonso, S, Valcarcel, Y. 2014. Phthalate occurrence in rivers and tap water from central Spain. *Science of the Total Environment*, 500-501: 139-146.

Han, S, Mao, D, Wang, H, Guo, H, 2022. An insightful analysis of dimethyl phthalate degradation by the collaborative process of DBD plasma and Graphene-WO_3 nanocomposites. Chemosphere, 291, 132774.

Guan, H, Liu, S, Duan, Y, Zhao, Y, 2007. Investigation of the electromagnetic characteristics of cement based composites filled with EPS. Cement and Concrete Composites, 29(1):49-54.

Li, S X, Lai, C, Li, C G, Zhong, J T, He, Z F, Peng, Q Y, Liu, X, Ke, B H, 2021. Enhanced photocatalytic degradation of dimethyl phthalate by magnetic dual Z-scheme iron oxide/mpg-C_3N_4/BiOBr/polythiophene heterostructure photocatalyst under visible light. Journal of Molecular Liquid, 342, 116947.

Li, D, Yu, J H, Jia, J L, He, H Y, Shi, W, Zheng, T, Ma, J, 2022. Coupling electrode aeration and hydroxylamine for the enhanced Electro-Fenton degradation of organic contaminant: Improving H_2O_2 generation, Fe^{3+}/Fe^{2+} cycle and N_2 selectivity. Water Research, 214: 118167.

Liu, S T, Chen, X G, Zhang, A B, Yan, K K, Ye, Y, 2014. Electromagnetic Performance of Rice Husk Ash. Bioresources, 9(2):2328-2340.

Mackintosh, CE, Maldonado, JA, Ikonomou, MG, Gobas, FAPC. 2006. Sorption of phthalate esters and PCBs in a marine ecosystem. Environmental Science & Technology, 40(11): 3481-3488.

Moučka, R, Mravčáková, M, Vilčáková, J, Omastová, M, Sáha, P, 2011. Electromagnetic absorption efficiency of polypropylene/montmorillonite/polypyrrole nanocomposites. Materials & Design, 32(4):2006-2011.

Net, S，Dumoulin, D, El-Osmani, R, Rabodonirina, S, Ouddane, B. 2014. Case Study of PAHs，Me-PAHs，PCBs，Phthalates and Pesticides Contamination in the Somme River Water, France. International Journal of Environmental Research, 8(4): 1159-1170．

Selvaraj, KK, Sundaramoorthy, G, Ravichandran, PK, Girijan, GK, Sampath, S, Ramaswamy, BR. 2015. Phthalate esters in water and sediments of the Kaveri River, India: environmental levels and ecotoxicological evaluations. Environmental Geochemistry and Health, Health, 37: (1): 83-96．

Shen, Y, Xu, Q, Yin, X, Wang, M, Zhang, N, Wu, S, Zhang, Z, Gu, Z, Wang, H. 2010. Determination and Distribution Features of Phthalate Esters in Xuanwu Lake. Journal of Southeast University (Natural Science Edition), 40 (6): 1337-1 341. (in Chinese)

Zeng, F, Cui, KY, Xie, ZY, Liu, M, Li, YJ, Lin, YJ, Zeng, ZX, Li, FB. 2008. Occurrence of phthalate esters in water and sediment of urban lakes in a subtropical city, Guangzhou, South China. Environment International, 34(3): 372-380.

Zhang, A., Liu, S., Yan, K., Ye, Y., Chen, X. 2014. Facile preparation of $MnFe_2O_4$/halloysite nanotubular encapsulates with enhanced magnetic and electromagnetic performances. *RSC Advances,* 4**,** 13565.